



This is a repository copy of *Lipidated DNA nanostructures target and rupture bacterial membranes*.

White Rose Research Online URL for this paper:

<https://eprints.whiterose.ac.uk/213328/>

Version: Published Version

Article:

Bennett, I.D., Burns, J.R., Ryadnov, M.G. et al. (2 more authors) (2024) Lipidated DNA nanostructures target and rupture bacterial membranes. *Small*, 20 (35). 2207585. ISSN 1613-6810

<https://doi.org/10.1002/sml.202207585>

Reuse

This article is distributed under the terms of the Creative Commons Attribution (CC BY) licence. This licence allows you to distribute, remix, tweak, and build upon the work, even commercially, as long as you credit the authors for the original work. More information and the full terms of the licence here:

<https://creativecommons.org/licenses/>

Takedown

If you consider content in White Rose Research Online to be in breach of UK law, please notify us by emailing eprints@whiterose.ac.uk including the URL of the record and the reason for the withdrawal request.



eprints@whiterose.ac.uk
<https://eprints.whiterose.ac.uk/>

Lipidated DNA Nanostructures Target and Rupture Bacterial Membranes

Isabel D. Bennett, Jonathan R. Burns, Maxim G. Ryadnov, Stefan Howorka,*
and Alice L. B. Pyne*

Chemistry has the power to endow supramolecular nanostructures with new biomedically relevant functions. Here it is reported that DNA nanostructures modified with cholesterol tags disrupt bacterial membranes to cause microbial cell death. The lipidated DNA nanostructures bind more readily to cholesterol-free bacterial membranes than to cholesterol-rich, eukaryotic membranes. These highly negatively charged, lipidated DNA nanostructures cause bacterial cell death by rupturing membranes. Strikingly, killing is mediated by clusters of barrel-shaped nanostructures that adhere to the membrane without the involvement of expected bilayer-puncturing barrels. These DNA nanomaterials may inspire the development of polymeric or small-molecule antibacterial agents that mimic the principles of selective binding and rupturing to help combat antimicrobial resistance.

1. Introduction

The ability to manipulate DNA into nanostructures of defined architecture by self-assembly has revolutionized the field of nanoengineering^[1–3] to achieve controlled biomolecular interactions with proteins or cellular surface markers.^[4–7] To interact with biological membranes, an array of DNA nanostructures have been designed over the past decade, including membrane-puncturing pores^[8–10] to transport cargo, and bilayer-floating DNA rafts^[11,12] to influence local bilayer composition and cytoskeleton-like structures that define the shape of lipid vesicles^[13–15] for biomedical applications.^[16] As novel classes of antimicrobials are urgently needed to help combat antimicrobial resistance (AMR),^[17] the antimicrobial activity of extracellular DNA has been tested,^[18,19] raising the possibility of nano-designed DNA structures that specifically interfere with bacterial membranes.^[20]

New nanoengineered DNA structures can complement well-documented antibacterial reagents, such as antimicrobial peptides. Antimicrobial peptides porate bacterial membranes to cause fractures and lesions resulting in cell death.^[21,22] The activity of antimicrobial peptides can be readily altered by introducing cationic and hydrophobic regions to transverse or disrupt negatively charged bacterial membranes.^[23] Antimicrobial peptides usually kill microorganisms at micromolar concentrations as the peptides must reach a threshold concentration in phospholipid bilayers, which enables their assembly into membrane-disrupting pores.^[24] In this process, individual peptide molecules undergo a conformational transition to form supramolecular structures that are stable and large enough to porate membranes. For example, Daptomycin, a natural lipo-peptide, assembles on the surface of Gram-positive bacteria mediated by calcium ions to form membrane pores and fractures.^[25] This drug is injected intravenously to selectively target pathogenic bacteria, and not erythrocytes, white blood cells, and other mammalian cell types. However, some antimicrobial peptides can be toxic, unstable, and require complicated and expensive synthesis. In addition, it can be challenging to develop new peptide iterations with improved therapeutic action to help overcome antimicrobial resistance.

Here we show that DNA nanobarrels carrying cholesterol lipid anchors target and rupture bacterial membranes (**Figure 1A,B**). The membrane activity of the barrels is demonstrated by

I. D. Bennett, A. L. B. Pyne
London Centre for Nanotechnology
University College London
17–19 Gordon Street, London WC1H 0AH, United Kingdom
E-mail: a.l.pyne@sheffield.ac.uk

I. D. Bennett
Division of Medicine
University College London, Cruciform Building
Gower Street, London WC1E 6BT, United Kingdom

J. R. Burns, S. Howorka
Department of Chemistry, Institute of Structural Molecular Biology
University College London
London WC1H 0AJ, United Kingdom
E-mail: s.howorka@ucl.ac.uk

M. G. Ryadnov
National Physical Laboratory
Teddington TW11 0LW, United Kingdom

M. G. Ryadnov
Department of Physics
King's College London
Strand Lane, London WC2R 2LS, United Kingdom

A. L. B. Pyne
Department of Materials Science and Engineering
University of Sheffield
Sir Robert Hadfield Building, Sheffield S1 3JD, United Kingdom

 The ORCID identification number(s) for the author(s) of this article can be found under <https://doi.org/10.1002/smll.202207585>

© 2024 The Authors. Small published by Wiley-VCH GmbH. This is an open access article under the terms of the [Creative Commons Attribution License](https://creativecommons.org/licenses/by/4.0/), which permits use, distribution and reproduction in any medium, provided the original work is properly cited.

DOI: 10.1002/smll.202207585

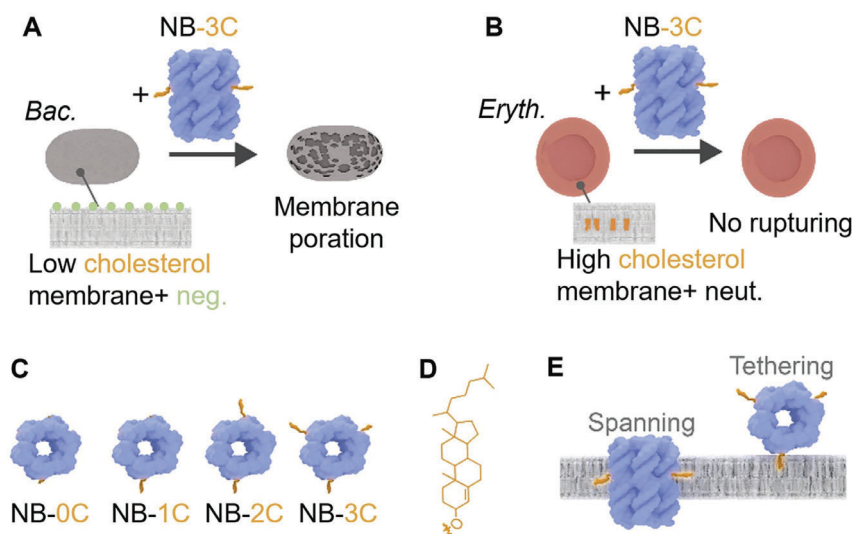


Figure 1. DNA nanobarrels with cholesterol membrane anchors and their interaction with model bacterial and erythrocyte membranes. A,B) Scheme of DNA-nanobarrels (NB) rupturing cholesterol-free bacterial membranes (B) but not cholesterol-rich erythrocyte cells. C) Top-down view of DNA nanobarrels NB-0C, and NB-1C to NB-3C carrying 1 to 3 cholesterol anchors, respectively. D) Structure of cholesterol lipid anchor used in this study. For endogenous cholesterol in bilayer membranes, the oxygen is bonded to hydrogen. For DNA-tethered cholesterol, the oxygen is attached to a chemical linker. E) The cholesterol tags help NBs span (left) or tether to the bilayer (right).

imaging of model membranes^[26–29] and living bacterial cells^[30–33] with high-resolution atomic force microscopy (AFM) and confocal laser scanning microscopy (CLSM). Membrane-active antimicrobials are a powerful route to combat antimicrobial resistance^[34–36] as several resistance-conferring mutations would have to arise against the multi-component biostructures for resistance to occur.^[37,38] Furthermore, selective action against bacterial membranes can be achieved by exploiting the unique biochemical content of bacterial membranes as achieved in nature by antimicrobial peptides that target anionic lipids in bacterial membranes.^[39–41]

2. Design and Formation of Cholesterol-Tagged DNA Nanobarrels

Our cholesterol-tagged DNA nanobarrels were rationally designed to target low-cholesterol bacterial membranes but not high-cholesterol eukaryotic membranes (Figure 1A,B) that are less dynamic due to the high cholesterol content.^[34,35,42] The DNA nanobarrels composed of six interconnected DNA duplexes (Figure 1C,D) were previously shown to bind to synthetic bilayers.^[10] Following our rational design, the hydrophobic cholesterol tags were expected to lead the negatively charged DNA structures to bind to cholesterol-free bacterial membranes (Figure 1A) via insertion of the cholesterol anchors into temporary structural membrane voids generated by the absence of endogenous cholesterol lipid in these bilayers. By contrast, cholesterol-tagged DNA nanostructures were anticipated to bind poorly to cholesterol-rich eukaryotic membranes (Figure 1B) given their more rigid bilayer nature. Within the preferred interaction, DNA nanobarrels were assumed to bind bacterial membranes either by spanning or tethering to lipid bilayers (Figure 1E).^[43] The differential interaction was explored with biological membranes of *E. coli* and human erythrocytes as well

as model membranes. The synthetic bacteria-mimicking membranes contained zwitterionic lipid phosphatidylethanolamine (PE) and negatively charged phosphatidylglycerol (Figure S1, Supporting Information) at a molar ratio of 80:20,^[44] while eukaryotic-mimicking membranes were composed of PE, zwitterionic phosphatidylcholine and cholesterol at a ratio of 15:35:50.^[45] The model membranes were deliberately devoid of other components, such as bacterial lipid polysaccharide or membrane proteins to test the influence of cholesterol in the membranes on DNA nanobarrel binding, as detailed further below.

To probe the influence of the number of cholesterol tags on membrane binding,^[46] DNA nanobarrels (NB) with zero, one, two, and three cholesterol anchors were used; NB-0C, NB-1C, NB-2C, and NB-3C, respectively (Figure 1C; Figures S2 and S3 and Tables S1 and S2, Supporting Information). The barrels were formed by self-assembly of six oligonucleotides carrying up to three cholesterol tags at the DNA strand termini (Figure S2,S3 and Table S1, Supporting Information). Assembly was confirmed by the observation of defined gel electrophoresis bands using both agarose and native PAGE, SDS was used to remove band smearing artifacts (Figure 2A; Figure S4, Supporting Information). The expected dimensions of these NBs of 5 nm x 9 nm (Figure S3, Supporting Information) were confirmed by AFM analysis of NB-0C adsorbed on mica. The structures had a height of $1.6 \text{ nm} \pm 0.3 \text{ nm}$, width of $5.5 \text{ nm} \pm 0.6 \text{ nm}$, and length $9.2 \text{ nm} \pm 0.8 \text{ nm}$ ($n = 11$) (Figure 2B; Figure S5, Supporting Information).

Membrane anchoring was achieved for barrels with at least one cholesterol tag as shown by gel electrophoretic analysis of barrels incubated with small unilamellar vesicles (SUVs). The gel band of the barrel was upshifted because the vesicles were unable to migrate into the gel matrix (Figure 2C).

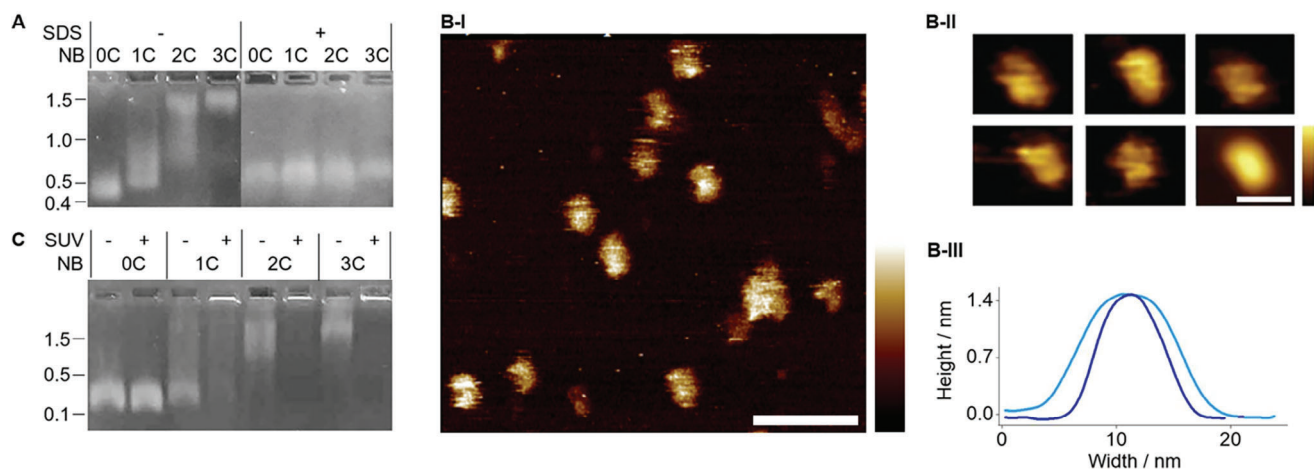


Figure 2. Structural characterization of DNA nanobarrels. A) Agarose gel electrophoretic analysis of NBs with up to three cholesterol anchors in the absence and presence of SDS detergent. The position and bp length of the dsDNA markers are shown on the left. B) Atomic force analysis of NB-0C, B-I) micrograph of wide view, scale bar 30 nm, vertical scale 2 nm, B-II) micrographs of individual NB-0C, bottom right image was obtained by correlation averaging of 11 nanobarrels, scale bar 10 nm, vertical scale 2 nm, B-III) line section profiles taken from averaged image showing the long (light blue) and short axis (dark blue) from averaged image in B-I. C) Agarose gel electrophoretic analysis of NBs with up to three cholesterol anchors in the absence and presence of SUVs. The position and bp length of the dsDNA markers are shown on the left.

3. Cholesterol Anchors Contribute to Antimicrobial Activity in Model Membranes

To determine the nature of the membrane interactions, nanobarrels containing a single cholesterol and the maximum number of three choles- terols were used. Due to the challenging nature of high-resolution AFM measurements on living cells, and the size disparity between bacterial cells and DNA nano- barrels, supported lipid bilayers were used to visualize nano- barrel distributions within model membranes that mimic the lipid composition of bacteria and erythrocyte membranes.^[45] The bare membrane, which was generated by spreading SUVs

onto mica, appeared flat in AFM analysis (Figure S6, Supporting Information). For studying DNA nanobarrel interaction, mem- brane vesicles were formed in the presence of DNA nano- structures followed by spreading the hybrid nanobarrel vesicles onto mica.

According to AFM analysis, DNA nanobarrels interacted with both negatively charged and zwitterionic membranes, however, an order of magnitude more nanobarrels were detected on bacterial membranes than erythrocyte membranes for NB-3C (Figure 3A) as shown by the volumes of elevations at $236 \times 10^3 \text{ nm}^3$ versus $15.6 \times 10^3 \text{ nm}^3$, respectively (Table S3, Supporting Information). Furthermore, nanobarrels at negatively charged

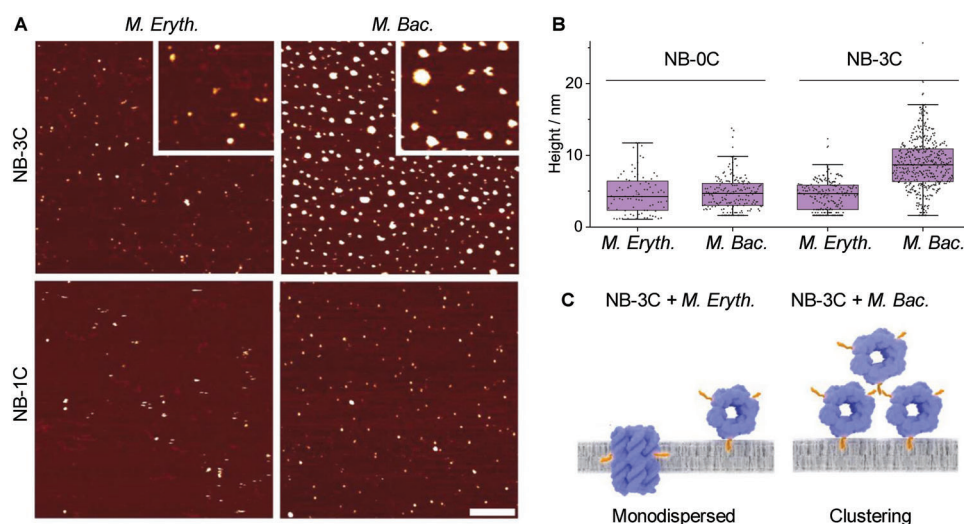


Figure 3. DNA nanobarrel NB-3C forms clusters on model bacterial membranes but not model erythrocyte bilayers. A) AFM micrographs of NB-3C (top row) and NB-1C (bottom row) to model membranes for erythrocytes (PE:PC:Chol) (left column) and bacteria (PE:PG) (right column). The scale bar for all images is 200 nm. B) Box plot of the elevations' mean radius identified in A. C) Schematic representation of NB-3C with erythrocyte membranes, which adopts a membrane-spanning or tethering alignment, or clustering arrangement for model bacterial membranes.

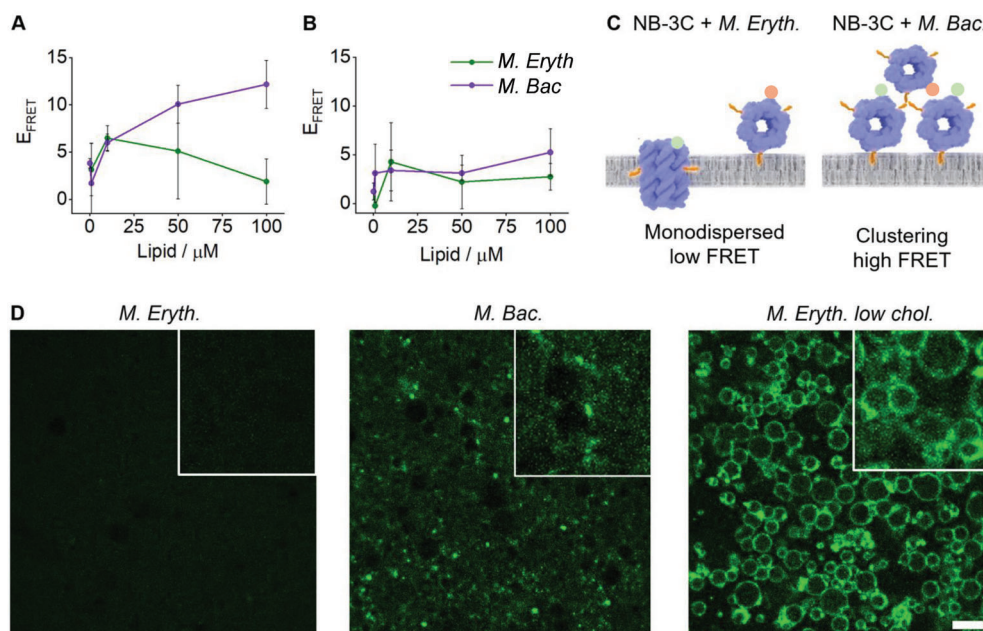


Figure 4. NB-3C clusters on vesicles composed of bacterial model membranes as shown by CLSM and FRET assays. A,B) Plot of E_{FRET} values for NB-3C (A) and NB-1C (B) with model SUVs for Gram-negative bacteria (violet) and erythrocytes (green). C) Schematic representation of an assay using FRET pair-labeled DNA NB-3C's, containing either a FAM (donor, green sphere) or Cy3 (acceptor, red sphere). Upon addition to SUVs, the barrels aggregate on the membrane surface giving rise to increased FRET intensity. D) CLSM images of FAM-labeled NB-3C with GUVs composed of either model erythrocyte GUVs, model bacteria GUVs, and model erythrocytes with no cholesterol. Scale bars 10 μm .

membranes were distributed as clusters (Figure 3A) of mean radius $8.8 \text{ nm} \pm 3.6 \text{ nm}$ (Figure S7 and Table S3, Supporting Information). These clusters were on average twice the dimensions of the protrusions observed for NB-3C in erythrocyte model membranes (mean radius $5 \text{ nm} \pm 2 \text{ nm}$, Figure 3B and $N = 199$) or for nanobarrels containing one cholesterol anchor, NB-1C (Figure S7 and Table S3, Supporting Information). The clustering of nanobarrels on bacterial model membranes is caused by membrane-tethered as opposed to membrane spanning nanobarrels (Figure 3C), as shown by removing of tethered barrels with the laterally sweeping AFM cantilever and rescanning (Figures S8 and S9, Supporting Information). The clustering mechanism is postulated to destabilize the negatively charged bacterial membrane and lead to increased cell death (see below). As a side note, nanobarrel clusters may also be present at the underside of the membrane however, it is not possible to observe this in the AFM experiments as the membranes are adhered to the mica surface and can only be explored from above.

The clustering of NB-3C on bacterial model membranes was confirmed by a fluorescence energy transfer (FRET) assay (Figure 4; Figure S10, Supporting Information). The nanobarrels were labelled with either a donor or acceptor fluorophore (Tables S1 and S2, Supporting Information) and combined in equimolar ratios. The pooled nanobarrels were then incubated with increasing concentrations of model bacterial or erythrocyte model membrane SUVs. Only NB-3C incubated with bacterial membranes exhibited increased FRET intensity at higher lipid concentrations, indicating clustering (Figure 4A,C). FRET intensity was not steady across all lipid concentrations but rather increased due to the partitioning of labeled NB-3C from solution to vesicle membranes at lower lipid concentration followed

by reaching a FRET plateau due to nanobarrel cluster formation even at high lipid concentrations. To determine if differential membrane interaction of nanobarrels and their clustering at bacterial membranes also occurs with preformed vesicles, we monitored nanobarrel binding toward giant unilamellar vesicles (GUVs) using CLSM. Using fluorophore-labeled constructs, we studied NB-3C and NB-0C binding toward GUVs containing model erythrocyte and model Gram-negative membranes (Figure 4D; Figure S11, Supporting Information). The insight from these images is consistent with the previous finding as NB-3C did not bind to the model erythrocyte GUVs but bound in aggregates to model Gram-negative GUVs. To help identify the role of cholesterol in the differential interaction between both model membranes, we decreased the concentration of cholesterol in the erythrocyte model membranes. The CLSM images strikingly revealed strong NB-3C binding to cholesterol-reduced erythrocyte membranes. These results confirm the central role of the cholesterol membrane content in dictating the binding of cholesterol-tagged nanobarrels under these conditions.

4. Cholesterol-Tagged Nanobarrels Induce Morphological Changes to Cause Cell Death in *E. coli*

Having established the interaction of nanobarrels with model membranes, the effect of the nanobarrels on *E. coli* cells was investigated. First, we monitored nanobarrel binding to *E. coli* and erythrocytes using CLSM (Figure 5A; Figure S12, Supporting Information). Using Cy3-labeled constructs, we observed NB-3C binding to GFP-labeled *E. coli* cells in both 1x phosphate-buffered saline (PBS) and 1x TAE 14 mM MgCl_2 but no NB-0C

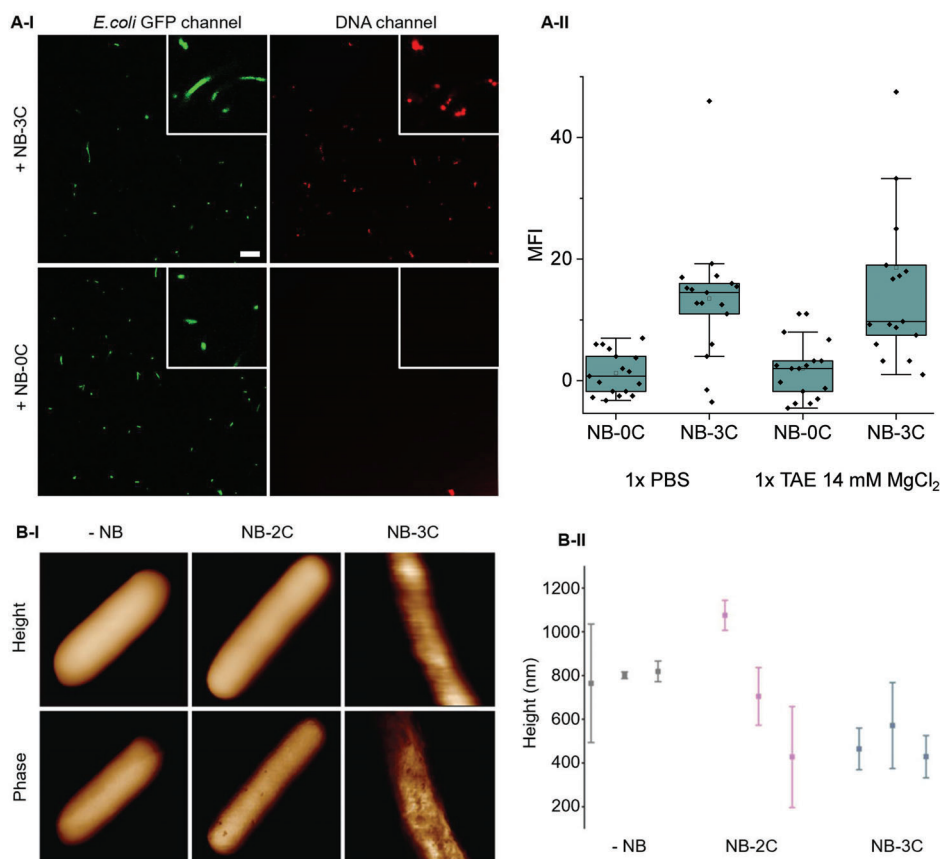


Figure 5. DNA nanobarrels disrupt *E. coli* cells. A-I) CLSM images of *E. coli* GFP with either NB-3C^{Cy3} or NB-0C^{Cy3}, scale bar 10 microns. A-II) Box plot of medium fluorescence intensities (MFI) of the stated construct either in PBS or 1x TAE 14 mM MgCl₂, $n = 20$. B-I) Representative AFM images showing the morphology for untreated and NB-2C or NB-3C treated *E. coli* cells ($n = 50, 8,$ and 7 bacteria for untreated, NB-2C, and NB-3C, respectively). B-II) Height distribution for untreated and for NB-2C or NB-3C treated *E. coli* cells, as determined from average peak height measurements shown in Figure S13 (Supporting Information). Error bars show width at $1/2$ peak height.

binding thereby confirming the requirement of the cholesterol tag for membrane binding. Almost all cells displayed NB-3C colocalization with *E. coli* cells indicating efficient membrane binding.

To explore nanobarrel interaction with living bacterial membranes, AFM was used to image live cells in solution that had been immobilized on a glass support (Figure 5B). High-resolution micrographs of entire bacteria showed untreated cells as smooth rods, and cells treated with NB-2C and NB-3C with pitted surfaces, that is, undergoing membrane disruption. For cells treated with NB-2C, the amount of membrane disruption varied across cells, with some cells showing a few deep pores, to more extensive membrane disruption. Cells treated with NB-3C displayed extensive membrane damage, with rupturing and blebbing observed on some cells (further examples shown in Figure S13, Supporting Information). The cell data highlights the membrane activity of barrels as a function of their number of membrane anchors.

Bacterial viability is closely linked to morphology, and as such, we characterized the level of membrane damage by measuring the height distributions of the cells (Figure 5B). Untreated cells (-NB, gray) presented with a cell height of $\approx 0.8 \mu\text{m}$, indicative of healthy cells. Cells treated with NB-2C (red) showed changes in

their cell height, indicating the cells were undergoing changes to their morphology and viability. Cells treated with NB-3C (green), showed a larger decrease in height of $\approx 0.5 \mu\text{m}$ compared to untreated cells, demonstrating significant cell damage. Error bars represent $1/2$ peak height, indicating to which degree the height of the bacterium varies within a single image. The spread of height distribution peaks for NB-2C both within a single bacterium and across the three images confirms the varied levels of membrane degradation seen in the AFM images. The variation may be due to local concentration differences of membrane-active NB-2C, or may indicate heterogeneity in the cells' sensitivity to attack by NB-2C. There is one anomalous cell height for one NB-2C cell, which appears to be $>1 \mu\text{m}$ (Figure 5B). This may be due to cell swelling in response to membrane disruption, which is a bacterial response to stress.^[39]

5. High-Resolution Imaging of Live *E. coli* Shows Cholesterol-Tagged Nanobarrels Cause Cell Death by Damaging the Bacterial Membrane

To probe whether the clustering of DNA nanobarrels NB-3C observed in model membranes results in increased

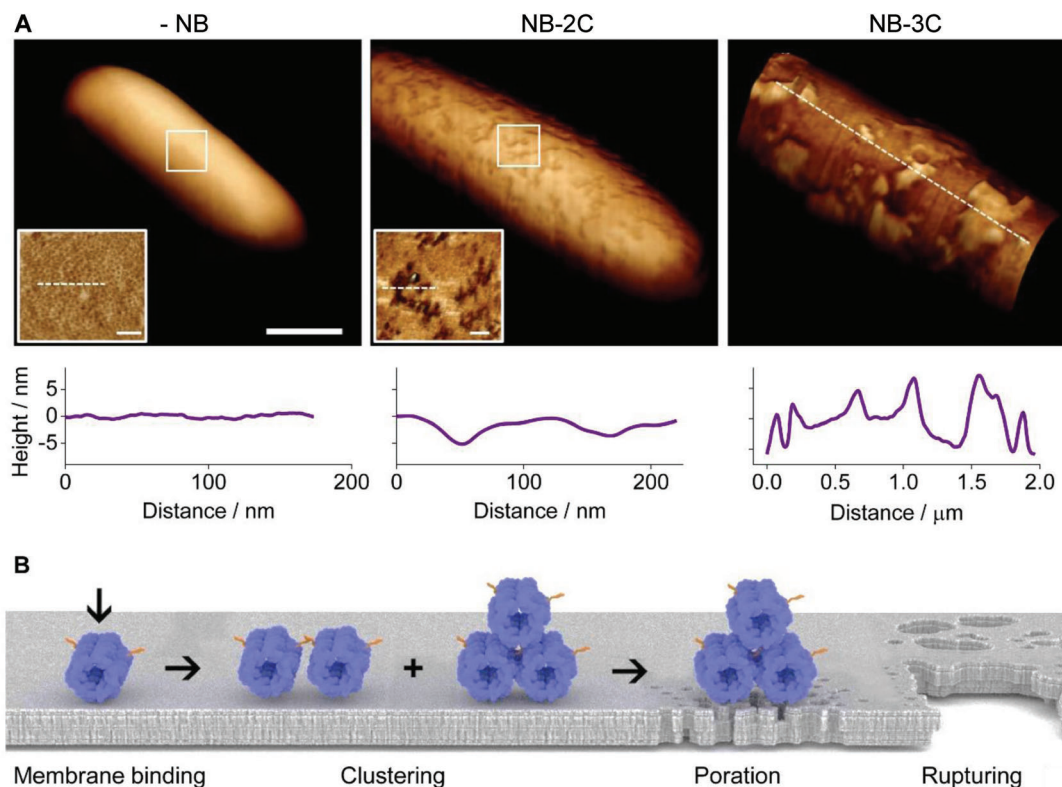


Figure 6. DNA nanobarrels rupture membranes of *E. coli* cells. A) AFM micrographs of *E. coli* cells prior to addition of NB (left), and after incubation with NB-2C (center), and NB-3C (right) at 37 °C, 300 nm. Cells were imaged at RT, data shown is height data with phase overlaid, insets show high-resolution micrographs of the boxed areas ($n = 20$ (-NB) and $n = 5$ (NB-2C)). Height line profiles (bottom) were taken along the white dashed lines. Scale bar: 500 nm, inset (left) 50 nm, (center) 100 nm. Vertical scale: (left) and (center) 900 nm, (right) 380 nm, insets 12 nm. B) Proposed mechanism of DNA nanobarrel binding to membranes, clustering, and membrane poration and rupturing.

nanobarrel-mediated membrane degradation in live bacteria, high-resolution micrographs of the surface of bacteria were taken (Figure 6). These showed marked differences in the outer membrane of bacteria which had been treated with 300 nm NB-3C nanobarrels as compared to untreated cells. High-resolution micrographs of untreated bacteria showed a smooth surface, with a characteristic pattern of shallow ≈ 7 nm-wide porin structures across the surface visible at higher resolution (Figure 6A, -NB, inset). On treatment with nanobarrels containing two cholesterol anchors (NB-2C), this surface was disrupted with large areas of membrane damage visible as $5 \text{ nm} \pm 1 \text{ nm}$ deep holes in the membrane surface (Figure 6A, NB-2C, inset and line profile). Nanobarrels containing three cholesterol anchors (NB-3C) exhibited higher activity than NB-2C, resulting in almost total removal of the outer membrane (Figure 6A, NB-3C), showing large steps of ≈ 15 nm visible in the height profile.

The greater membrane disruption observed on treatment with NB-3C suggests the third cholesterol increases membrane activity. This extra cholesterol may allow NBs to bind together on the membrane forming clusters or a DNA lattice, which together cause greater membrane disruption than dispersed NBs. The cholesterol anchors could also cluster together forming lipid rafts, often observed in biological membranes^[36] (Figure 6B). We do however note that these studies were carried out in low

salt buffers, which may have aided the membrane activity of the nanobarrels by osmotically destabilizing the cells. Low salt was required to obtain good adhesion of the bacterial cells to the substrate for AFM measurements, and for achieving high-resolution measurements. Our experimental results effectively demonstrate that DNA barrels can damage bacterial membranes, which may lead to bacterial cell death.

In line with the proposed selectivity against cholesterol-poor bacteria, nanobarrel NB-3C displayed negligible binding to red blood cells with cholesterol-rich membranes. Bovine erythrocytes (Table 1) showed only minimal binding, change of cell morphology, or membrane disruption when exposed to 500 nm NB-3C (Figure S14, Supporting Information). Red blood cells are usually very sensitive to bilayer rupturing agents.^[47,48] The non-disruptive behavior of the cholesterol-modified NB against erythrocytes and other cells has also been observed in a previous study^[48] even though other types of membrane-anchors can lead to cell toxicity.^[49]

Table 1. Haemolysis assay.

Reagent	H ₂ O	PBS	NB-0C	NB-1C	NB-3C
% haemolysis	100	0	0.17	0.17	0.69

6. Conclusion

This study is the first to engineer lipidated DNA nanostructures that kill bacterial cells thereby addressing the growing demand for functional and biologically active DNA nanomaterials, as well as the need for new chemical approaches to target bacterial membranes to help overcome antimicrobial resistance. Our high-resolution AFM and fluorescence microscopy studies on bacterial cells revealed that the engineered DNA-lipid nanobarrels disrupt the negatively charged bacterial membrane, causing extensive membrane disruption and cell death at nanomolar concentrations. This disruption is facilitated by cholesterol anchors which selectively target bacterial and biomimetic membrane which are poor in endogenous cholesterol. The membrane-rupturing ability of the DNA nanobarrels can be tuned by changing the number of cholesterol anchors from two to three – corresponding to a mass change of solely 0.4%. Removing the cholesterol anchors stops the membrane-rupturing activity entirely.

DNA nanobarrels offer a new approach to design membrane-rupturing agents with a high degree of structural programmability, at the price of a smaller spectrum of chemical diversity compared to other antimicrobial agents such as antimicrobial peptides. Within this design space, we have shown that DNA nanobarrels can selectively target bacterial membranes via cholesterol anchors that interact with cholesterol-poor membranes with negative headgroups and form DNA barrel clusters to rupture membranes. Further studies can exploit the modularity of the DNA-based rational design approach to build increasingly more active and biocompatible nanostructures. This strategy includes screening arrays of diverse nanostructures with different dimensions and orientations,^[50] introducing alternative hydrophobic functional groups to identify the optimal targeted therapeutic action,^[51] and employing coating agents to improve biocompatibility and improve nuclease stability, such as oligolysine^[52] and albumin^[53] molecules. A far-reaching yet equally exciting route will be the development of smaller organic compounds that mimic structural/functional aspects of the DNA barrels such as cholesterol membrane anchors or negatively charged small molecules. In conclusion, our antimicrobial DNA nanostructures advance functional and applied DNA nanotechnology and may inspire new antimicrobial agents aimed at overcoming resistance against existing antibiotics.

7. Experimental Section

Materials: Native and cholesterol-labeled DNA oligonucleotides were procured from Integrated DNA Technologies(UK) on a 1 μmol scale with HPLC or PAGE purification. 1,2-dioleoyl-sn-glycero-3-phosphoethanolamine (DOPE), 1,2-dioleoyl-sn-glycero-3-phosphocholine (DOPC) and 1,2-dioleoyl-sn-glycero-3-phospho-rac-(1-glycerol) sodium salt (DOPG) (Figure S3, Supporting Information) were obtained from Avanti Polar Lipids (UK). All other reagents and solvents were purchased from Sigma-Merck (UK) unless stated otherwise.

Assembly of DNA Nanostructures: An equimolar mixture of DNA oligonucleotides (1 nmol each, dissolved in 1x PBS, total volume 1,000 μL , unless stated otherwise) was prepared at RT, incubated at 95 $^{\circ}\text{C}$ for 2 min, and cooled to 20 $^{\circ}\text{C}$ at a rate of 5 $^{\circ}\text{C min}^{-1}$ using a PCR thermocycler (Bio-Rad, UK).

Gel Electrophoresis: The assembled DNA barrels were analyzed using either 1.3% agarose gel using TAE buffer pH 8.0 with or without 0.015% v/v SDS. A solution containing 5 pmol DNA was mixed with 5 μL blue gel loading dye before transferring the solution into wells. The gel was run at

70 V for 60 min at RT. The bands were visualized by ultraviolet illumination after staining with ethidium bromide solution. SDS containing gels were washed with deionized water for 20 min prior to staining. A 100-base-pair marker (New England Biolabs, UK) was used as the reference standard.

For agarose gel electrophoretic analysis of the interaction of nanobarrels with small unilamellar vesicles (SUVs), the same gel conditions as described above were used in the absence of SDS. Furthermore, the barrels (15 μL , 1 μM , 0.3 M KCl, 15 mM Tris pH 8.0) were incubated with SUVs (15 μL , 1 mM, 0.3 M KCl, 15 mM Tris pH 8.0) for 30 min at 37 $^{\circ}\text{C}$, followed by the addition of blue loading dye (6x, no SDS, 10 μL), and loading onto the gel (10 μL).

For native PAGE analysis, the same conditions above were used, except a 4–20% PAGE gel (Bio-Rad, USA) was employed, and the gel was conducted in pre-equilibrated 1x TBE buffer at 4 $^{\circ}\text{C}$. A 100-base-pair marker (New England Biolabs, UK) was used as the reference standard. The bands were visualized by ultraviolet illumination after staining with ethidium bromide solution.

Vesicle Formation—Formation of SUVs for Gel Analysis: Chloroform solutions of DOPE (13.4 mmolar, 50 μL), DOPC (12.7 mmolar, 550 μL), (Figure S3, Supporting Information) were combined. The lipid mixtures were added to an over-dried round bottom flask (10 mL), and the solvent was removed under vacuum using a rotary evaporator for 20 min, after which the thin film was dried under ultrahigh vacuum for 3 h. A solution of 0.3 M KCl, 15 mM Tris, pH 8.0 (1 mL) was added, and the suspension was sonicated for 20 min at RT. The generated SUVs were stored in the fridge and used within 1 week. Before experimentation, the SUV suspension was vortexed for 2 s. SUVs were subjected to dynamic light scattering (DLS) to confirm the diameters of the vesicles. DLS analysis was carried out on a Zetasizer Nano (ZEN3600, Malvern Instruments, UK) in a 100 μL disposable cuvette at 25 $^{\circ}\text{C}$. No sample filtration was carried out before the measurements so that vesicle populations remained unaffected. Hydrodynamic radii were obtained through the fitting of autocorrelation data to a single exponential function using the manufacturer's Dispersion Technology Software (DTS version 5.10).

Vesicle Formation—Formation of Large Unilamellar Vesicles (GUVs) for Atomic Force Microscopy (AFM) Analysis: Lipids DOPE (0.15 μmol , 25 μL), DOPC (0.35 μmol , 275 μL), and cholesterol (0.1 μmol , 20 μL) in chloroform were combined to create model eukaryotic membranes,^[54] and lipids DOPE (0.4 μmol , 150 μL) and DOPG (0.1 μmol , 37.8 μL) in chloroform were mixed to obtain model bacterial membranes.^[44] The solutions were added to a 10 mL over-dried round bottom flask, to which methanol (10 μL) and NB-3C or NB-1C (150 μL , 1 μM in 0.3 M KCl, 15 mM Tris, pH 8.0) was added. To generate LUVs with embedded nanobarrels, the organic solvent was removed under vacuum using a rotary evaporator for 2 min leaving only the aqueous phase.^[55] Afterward, the sample was transferred to a 1 mL plastic vial and centrifuged at 1,000 rpm for 30 s to remove any precipitate. Agarose gel electrophoresis and fluorescence analysis confirmed the presence of nanobarrels in the supernatant. The supernatant was subsequently used for AFM analysis.

Vesicle Formation—Formation of SUVs for Fluorescence Resonance Energy Transfer (FRET) Studies: Lipids DOPE (0.15 μmol , 25 μL), DOPC (0.35 μmol , 275 μL), and cholesterol (0.1 μmol , 20 μL) in chloroform were combined to create model eukaryotic membranes,^[54] and lipids DOPE (0.4 μmol , 150 μL) and DOPG (0.1 μmol , 37.8 μL) in chloroform were mixed to obtain model bacterial membranes using the protocol described above. The suspension was sonicated for 20 min at RT to generate SUVs. The vesicles were used within 24 h and resuspended by vortexing for 10 s prior to use.

Vesicle Formation—Formation of Giant Unilamellar Vesicles (GUVs) for Confocal Laser Scanning Microscopy (CLSM) Analysis: The GUVs were prepared by modifying a published protocol.^[15] Lipids DOPE (0.15 μmol , 25 μL), DOPC (0.35 μmol , 275 μL), and cholesterol (0.1 μmol , 20 μL) in chloroform were combined to create model eukaryotic membranes,^[54] and lipids DOPE (0.4 μmol , 150 μL) and DOPG (0.1 μmol , 37.8 μL) in chloroform were mixed to obtain model bacterial membranes.^[44] For the low cholesterol version of model eukaryotic membrane reduced cholesterol (0.025 μmol , 5 μL) in chloroform was used instead. The stated solutions

were then added to a glass vial (1 mL), and the solvent was removed under vacuum using a rotary evaporator for 5 min. The thin film generated was resuspended in mineral oil (150 μ L, M5904, lot number MKBX0231V) by vortexing and sonicating for 1 min. Sucrose (30 μ L, 400 mM) was added to the mineral oil layer and the suspension vortexed for 1 min at RT, then carefully added to the top of a glucose solution (1 mL, 400 mM) in a plastic vial (1 mL). The vesicles were generated by centrifuging at 14,100 \times g for 30 s. The mineral oil top layer and the majority of the sucrose layer (850 μ L) were carefully removed. The remaining solution containing the pelleted vesicles (100 μ L) was gently mixed with a pipettor, then transferred to a clean plastic vial and used within 24 h.

FRET Analysis of DNA Barrels and Their Interaction with Model Membranes: 5'-6-Fluorescein (FAM) and Cy3-labeled NB-3C, and FAM and Cy3-labeled NB-0C constructs were combined in equal ratios (50 μ L, 1 μ M each) and then added to the stated SUVs (100 μ L, 0–100 μ M lipid in 0.3 M KCl, 15 mM Tris, pH 8.0) and mixed for 10 min at RT. The suspension (125 μ L) was transferred to a fluorescent cuvette and the donor emission was determined by excitation at 495 nm and scanning the emission from 505 to 700 nm using a medium PMT voltage setting. The donor emission percentage was quantified according to the below equation:

$$E_{\text{FRET}} = (1 - \text{combined donor-acceptor emission/donor emission}) \times 100 \quad (1)$$

CLSM Analysis of DNA Barrels and Their Interaction with Model Membranes: The stated fluorescently-labeled nanobarrel construct (2 μ L, 1 μ M) was added to the stated GUV solution (5 μ L). Images were collected using a 60 \times oil objective CLSM (FV-1000 Olympus, UK). The samples were deposited on a fluorodish (FD35-100, World Precision Instruments, Sarasota, FL, USA) and left to settle for 5 min before imaging unless stated. Microscope settings were kept identical for each experiment where appropriate. Images were analyzed using ImageJ^[56] software (<https://imagej.nih.gov>).

AFM Analysis of DNA Barrels and Their Interaction with Model Membranes: For AFM analysis of non-membrane bound DNA barrels, NB-0C was adsorbed onto mica following a published procedure that uses Ni²⁺ cations for immobilization by bridging the negative charges of DNA and the mica substrate.^[57,58] To freshly cleaved mica, a solution of 10 mM Tris-HCl, 10 mM NiCl₂ pH 7.4 (49 μ L), and NB-3C (1 μ M in 0.3 M KCl, 15 mM Tris, pH 8.0, 1 μ L) was added and incubated for 1 h. The solution was diluted further in 10 mM Tris-HCl pH 7.4 to a final NiCl₂ concentration of \approx 2 mM for imaging. AFM topographical images of the nanobarrels were acquired in fluid at RT using a Multimode 8 Atomic Force Microscope (Bruker Santa Barbara, CA, USA) operated in tapping mode using a Biolever mini cantilever (Olympus, Japan). Imaging was performed at a set-point of 108 mV (\approx 2 nm) which was chosen to minimize imaging force whilst allowing clear tracking of the nanobarrels at 4 Hz line rates. For the analysis of individual nanobarrels, the image size was kept to 166 nm or less at a resolution of 512 pixels, resulting in a maximum pixel size of 0.35 nm pixel⁻¹. Images were processed using Gwyddion^[59] (<http://gwyddion.net/>) for line-by-line flattening and removal of tilt using a first-order polynomial. The color scale^[58] was set to 2 nm to show the individual nanobarrels against the background. Individual nanobarrels were cropped from the original image. An averaged image of the nanobarrels was obtained using the correlation averaging function in Gwyddion over 11 nanobarrels.

For AFM analysis of how NB-3C and NB-1C interact with model eukaryotic and bacterial membranes, freshly cleaved mica surfaces were incubated with a mixture of 10 mM MgCl₂, 10 mM CaCl₂, 10 mM Tris-HCl, pH 7.4 (49 μ L) and supernatant of LUVs co-formed with nanobarrels (1 μ L, \approx 1 μ M NB-3C or NB-1C, \approx 1 mM lipid) following a published procedure. The solution was left to adsorb for 1 h followed by exchanging the buffer 5 times to remove any unbound vesicles. AFM topographical images of the nanobarrels were acquired in fluid at RT using a FastScan Bio Atomic Force Microscope (Bruker Santa Barbara, CA, USA) operated in PeakForce Tapping mode using a FastScan D cantilever (Bruker Santa Barbara, CA, USA). Imaging was performed at a set-point of 0.008 V (\approx 40 pN) at a PeakForce frequency of 8 kHz with a 10 nm PeakForce amplitude. Each

experiment was repeated at least 3 times. For geometrical analysis of the nanobarrel populations in model membranes, the images were processed as above in Gwyddion. Any protrusions from the membrane were selected by height using the masking function in Gwyddion. Each singular masked object was then analyzed to determine its maximum height, mean radius, and volume (using a Laplacian interpolation) in Gwyddion. This data was processed in Origin to determine mean values and standard deviation and plotted as histograms.

AFM Analysis of Bacterial Cells Exposed to DNA Nanobarrels: Bacteria were immobilized on glass slides according to the following protocol. Briefly, *E. coli* JM109 cells (Promega, UK) were grown overnight in LB medium at 37 °C under shaking at 250 rpm. The culture was then diluted 1:100 and re-grown at 37 °C and 250 rpm for 3 h to reach an exponential growth phase. Bacteria were washed 3 \times with deionized water using intermittent sedimentation via centrifugation (5000 rpm, 2 min). Washed bacteria were bound to glass coverslips coated with 0.01% poly-L-lysine (Sigma–Aldrich, St Louis, USA) by incubation for 30 min at RT. The coverslips were then rinsed with water whereby care was taken to keep the bacteria wet. Bacteria bound to coverslips were then incubated with a solution of nanobarrels (300 nm, 0.1 \times PBS buffer) optionally carrying an Alexa647 dye. Bacteria incubated with NB-2C were imaged after 30 min and those with NB-3C after 20 min. Prior to imaging, the buffer was exchanged to 66 mM phosphate buffer saline (PB). Imaging was performed on a JPK Nanowizard Ultraspeed (JPK, DE). Topographic images of *E. coli* cells in liquid were recorded on a Nanowizard III AFM with an UltraSpeed head (JPK, DE) operated in intermittent contact mode at RT. The AFM probes used for experiments in liquid were FastScan-D (0.25 N m⁻¹) (Bruker AXS, CA, USA).

Images were processed using Gwyddion^[59] (<http://gwyddion.net/>) for 0th-order line-by-line flattening to center data, and 1st or 2nd-order plane fitting to remove tilt or bow. Phase data were overlaid onto the height data for Figure 3 using the 3D function in Gwyddion. High-resolution scans of *E. coli* membranes were processed using an additional 2nd-order polynomial fit to remove the curvature of the surface. Cross-section analysis was carried out using Gwyddion and plotted using Origin (OriginLab, MA, USA). The height distribution for each image was calculated using the 1D statistical functions tool in Gwyddion. A Gaussian multi-peak function was fitted to the data in Origin. Peak-to-peak height was taken as the height distribution peak of the bacterium. Full-width-at-half-maximum for both peaks were added together and plotted as error bars. When imaging compromised bacteria in tapping mode, the background surface was not always fully tracked hence full cell height may be underestimated. The micrographs of *E. coli* display representative results found in at least 3 independent experiments for 50 bacteria not incubated with nanobarrels, and 8 and 7 bacteria incubated with NB-2C and NB-3C, respectively.

CLSM Analysis of Bacterial Cells Exposed to DNA Nanobarrels: The stated Cy3 DNA nanobarrel construct (1 μ L, 1 μ M) was added to *E. coli*-GFP cells (10 μ L in PBS, stock optical density at 600 nm 1.0) and left to incubate for 90 min. The solution was mixed and then deposited (10 μ L) onto a fluorodish (FD35-100, World Precision Instruments, Sarasota, FL, USA) and left to settle for 5 min before imaging. For *E. coli* GFP, the same fermentation conditions as used for JM109 above were applied except the media was supplemented with kanamycin (10 μ g mL⁻¹), and IPTG (1 mM) was added to express GFP for 6 h prior to CLSM studies.

Haemolysis Assay: Haemolysis was determined by incubating 10% (v/v) suspension of bovine erythrocytes (Seralab, UK) with DNA barrels. Erythrocytes were washed 4 times in 1 \times PBS, pH 7.2, by repeated centrifugation and re-suspension (3 min at 3000 \times g). The washed erythrocytes (100 μ L) were incubated in a 96-well plate at RT for 1 h in either 100 μ L of deionized water, 1 \times PBS or with DNA constructs in 1 \times PBS (0.5 μ M final concentration). After centrifugation at 10,000 g for 5 min, the supernatant (150 μ L) was separated from the pellet and transferred into a new 96-well plate and the absorbance was measured at 550 nm using a FluoStar plate reader (BMG LabTech, DE). Absorbance of the suspension treated with deionized water defined complete haemolysis. The values correspond to the percentage of haemolysis at tested concentrations. All tests were done in triplicate.

Supporting Information

Supporting Information is available from the Wiley Online Library or from the author.

Acknowledgements

The authors acknowledge the EPSRC (EP/N009282/1), the BB-SRC (BB/M012700/1, BB/M025373/1, BB/N017331/1) the MRC (MR/R024871/2), and UKRI (MR/W00738X/1) for funding. The authors acknowledge the EPSRC IRC in Early-Warning Sensing Systems for Infectious Diseases (EP/K031953/1) for use of research facilities. The authors thank Elena Georgiou and MoMo Zandieh for critically reading the manuscript.

Conflict of Interest

The authors declare no conflict of interest.

Data Availability Statement

Data available in open repository with <https://doi.org/10.15131/shef.data.25662963>.

Keywords

antimicrobial resistance, atomic force microscopy, bacteria, DNA nanotechnology, DNA origami

Received: December 5, 2022

Revised: March 1, 2024

Published online:

- [1] P. W. Rothmund, *Nature* **2006**, *440*, 297.
- [2] F. Hong, F. Zhang, Y. Liu, H. Yan, *Chem. Rev.* **2017**, *117*, 12584.
- [3] N. C. Seeman, H. F. Sleiman, *Nat. Rev. Mater.* **2018**, *3*, 17068.
- [4] A. J. Wollman, C. Sanchez-Cano, H. M. Carstairs, R. A. Cross, A. J. Turberfield, *Nat. Nanotechnol.* **2014**, *9*, 44.
- [5] B. Sacca, C. M. Niemeyer, *Chem. Soc. Rev.* **2011**, *40*, 5910.
- [6] M. You, Y. Lyu, D. Han, L. Qiu, Q. Liu, T. Chen, C. Sam Wu, L. Peng, L. Zhang, G. Bao, W. Tan, *Nat. Nanotechnol.* **2017**, *12*, 453.
- [7] C. Sigl, E. M. Willner, W. Engelen, J. A. Kretzmann, K. Sachenbacher, A. Liedl, F. Kolbe, F. Wilsch, S. A. Aghvami, U. Protzer, M. F. Hagan, S. Fraden, H. Dietz, *Nat. Mater.* **2021**, *20*, 1281.
- [8] M. Langecker, V. Arnaud, T. G. Martin, J. List, S. Renner, M. Mayer, H. Dietz, F. C. Simmel, *Science* **2012**, *338*, 932.
- [9] J. R. Burns, E. Stulz, S. Howorka, *Nano Lett.* **2013**, *13*, 2351.
- [10] J. R. Burns, A. Seifert, N. Fertig, S. Howorka, *Nat. Nanotechnol.* **2016**, *11*, 152.
- [11] J. List, M. Weber, F. C. Simmel, *Angew. Chem., Int. Ed.* **2014**, *53*, 4236.
- [12] A. Johnson-Buck, S. Jiang, H. Yan, N. G. Walter, *ACS Nano* **2014**, *8*, 5641.
- [13] Y. Yang, J. Wang, H. Shigematsu, W. Xu, W. M. Shih, J. E. Rothman, C. Lin, *Nat. Chem.* **2016**, *8*, 476.
- [14] W. Xu, B. Nathwani, C. Lin, J. Wang, E. Karatekin, F. Pincet, W. Shih, J. E. Rothman, *J. Am. Chem. Soc.* **2016**, *138*, 4439.
- [15] N. Arulkumar, M. Singer, S. Howorka, J. R. Burns, *Nat. Commun.* **2023**, *14*, 1314.
- [16] Y. J. Chen, B. Groves, R. A. Muscat, G. Seelig, *Nat. Nanotechnol.* **2015**, *10*, 748.
- [17] J. M. V. Makabenta, A. Nabawy, C. H. Li, S. Schmidt-Malan, R. Patel, V. M. Rotello, *Nat. Rev. Microbiol.* **2021**, *19*, 23.
- [18] T. W. Halverson, M. Wilton, K. K. Poon, B. Petri, S. Lewenza, *PLoS Pathog.* **2015**, *11*, e1004593.
- [19] H. Mulcahy, L. Charron-Mazenod, S. Lewenza, *PLoS Pathog.* **2008**, *4*, e1000213.
- [20] I. Mela, P. P. Vallejo-Ramirez, S. Makarchuk, G. Christie, D. Bailey, R. M. Henderson, H. Sugiyama, M. Endo, C. F. Kaminski, *Angew. Chem., Int. Ed.* **2020**, *59*, 12698.
- [21] Q.-Y. Zhang, Z.-B. Yan, Y.-M. Meng, X.-Y. Hong, G. Shao, J.-J. Ma, X.-R. Cheng, J. Liu, J. Kang, C.-Y. Fu, *Mil. Med. Res.* **2021**, *8*, 48.
- [22] B. H. Gan, J. Gaynard, S. M. Rowe, T. Deingruber, D. R. Spring, *Chem. Soc. Rev.* **2021**, *50*, 7820.
- [23] C. D. Fjell, J. A. Hiss, R. E. W. Hancock, G. Schneider, *Nat. Rev. Drug Discovery* **2012**, *11*, 37.
- [24] K. Hammond, F. Cipcigan, K. Al Nahas, V. Losasso, H. Lewis, J. Cama, F. Martelli, P. W. Simcock, M. Fletcher, J. Ravi, P. J. Stansfeld, S. Pagliara, B. W. Hoogenboom, U. F. Keyser, M. S. P. Sansom, J. Crain, M. G. Ryadnov, *ACS Nano* **2021**, *15*, 9679.
- [25] W. R. Miller, A. S. Bayer, C. A. Arias, *Cold Spring Harbor Perspect. Med.* **2016**, *6*, a026997.
- [26] Y. Suzuki, M. Endo, H. Sugiyama, *Nat. Commun.* **2015**, *6*, 8052.
- [27] Q. Shen, M. W. Grome, Y. Yang, C. Lin, *Adv. Biosyst.* **2020**, *4*, 1900215.
- [28] A. Khmelinskaia, H. G. Franquelim, R. Yaadav, E. P. Petrov, P. Schwille, *Adv. Mater. Interfaces* **2021**, *8*, 2101094.
- [29] K. N. Baumann, L. Piantanida, J. Garcia-Nafria, D. Sobota, K. Voitchovsky, T. P. J. Knowles, S. Hernandez-Ainsa, *ACS Nano* **2020**, *14*, 2316.
- [30] H. Yamashita, A. Taoka, T. Uchihashi, T. Asano, T. Ando, Y. Fukumori, A. F. M. High-Speed, *J. Mol. Biol.* **2012**, *422*, 300.
- [31] A. Viljoen, S. J. Foster, G. E. Fantner, J. K. Hobbs, Y. F. Dufrene, *Scratching Surface: Bacterial Cell Envelopes Nanoscale* **2020**, *11*, 10.
- [32] D. A. Heesterbeek, B. W. Bardoel, E. S. Parsons, I. Bennett, M. Ruyken, D. J. Doorduyn, R. D. Gorham, E. T. Berends, A. L. Pyne, B. W. Hoogenboom, S. H. Rooijackers, *EMBO J.* **2019**, *38*, 99852.
- [33] L. Pasquina-Lemonche, J. Burns, R. D. Turner, S. Kumar, R. Tank, N. Mullin, J. S. Wilson, B. Chakrabarti, P. A. Bullough, S. J. Foster, J. K. Hobbs, *Nature* **2020**, *582*, 294.
- [34] R. E. W. Hancock, H.-G. Sahl, *Nat. Biotechnol.* **2006**, *24*, 1551.
- [35] L. L. Ling, T. Schneider, A. J. Peoples, A. L. Spoering, I. Engels, B. P. Conlon, A. Mueller, T. F. Schäberle, D. E. Hughes, S. Epstein, M. Jones, L. Lazarides, V. A. Steadman, D. R. Cohen, C. R. Felix, K. A. Fetterman, W. P. Millett, A. G. Nitti, A. M. Zullo, C. Chen, K. Lewis, *Nature* **2015**, *517*, 455.
- [36] C. D. Fjell, J. A. Hiss, R. E. Hancock, G. Schneider, *Nat. Rev. Drug Discovery* **2011**, *11*, 37.
- [37] J. M. Blair, M. A. Webber, A. J. Baylay, D. O. Ogbolu, L. J. Piddock, *Nat. Rev. Microbiol.* **2015**, *13*, 42.
- [38] P. R. Gonzales, M. W. Pesesky, R. Bouley, A. Ballard, B. A. Bidy, M. A. Suckow, W. R. Wolter, V. A. Schroeder, C.-A. D. Burnham, S. Mobashery, M. Chang, G. Dantas, *Nat. Chem. Biol.* **2015**, *11*, 855.
- [39] S. Mukherjee, H. Zheng, M. G. Derebe, K. M. Callenberg, C. L. Partch, D. Rollins, D. C. Prophet, J. Rizo, M. Grabe, Q.-X. Jiang, L. V. Hooper, *Nature* **2014**, *505*, 103.
- [40] X. Wang, D. M. Lord, H.-Y. Cheng, D. O. Osbourne, S. H. Hong, V. Sanchez-Torres, C. Quiroga, K. Zheng, T. Herrmann, W. Peti, M. J. Benedik, R. Page, T. K. Wood, *Nat. Chem. Biol.* **2012**, *8*, 855.
- [41] S. J. Lam, N. M. O'Brien-Simpson, N. Pantarat, A. Sulistio, E. H. H. Wong, Y.-Y. Chen, J. C. Lenzo, J. A. Holden, A. Blencowe, E. C. Reynolds, G. G. Qiao, *Nat. Microbiol.* **2016**, *1*, 16162.
- [42] J. Friedrichs, R. Helbig, J. Hilsenbeck, P. R. Pandey, J.-U. Sommer, L. D. Renner, T. Pompe, C. Werner, *Nature* **2023**, *618*, 733.

- [43] S. L. Veatch, S. L. Keller, *Phys. Rev. Lett.* **2002**, *89*, 268101.
- [44] R. F. Epand, P. B. Savage, R. M. Epand, *Biomembranes* **2007**, *1768*, 2500.
- [45] G. van Meer, D. R. Voelker, G. W. Feigenson, *Nat. Rev. Mol. Cell Biol.* **2008**, *9*, 112.
- [46] J. K. D. Singh, E. Darley, P. Ridone, J. P. Gaston, A. Abbas, S. F. J. Wickham, M. A. B Baker, *Nucleic Acids Res.* **2021**, *49*, 10835.
- [47] M. Hartmann, M. Berditsch, J. Hawecker, M. F. Ardakani, D. Gerthsen, A. S. Ulrich, *Antimicrob. Agents Chemother.* **2010**, *54*, 3132.
- [48] N. Arulkumaran, C. Lanphere, C. Gaupp, J. R. Burns, M. Singer, S. Howorka, *ACS Nano* **2021**, *15*, 4394.
- [49] J. R. Burns, N. Al-Juffali, S. M. Janes, S. Howorka, *Angew. Chem., Int. Ed.* **2014**, *53*, 12466.
- [50] C. Lanphere, D. Offenbartl-Stiegert, A. Dorey, G. Pugh, E. Georgiou, Y. Xing, J. R. Burns, S. Howorka, *Nat. Protoc.* **2021**, *16*, 86.
- [51] S. Huo, H. Li, A. J. Boersma, A. Herrmann, *Adv. Sci.* **2019**, *6*, 1900043.
- [52] N. Ponnuswamy, M. M. C. Bastings, B. Nathwani, J. H. Ryu, L. Y. T. Chou, M. Vinther, W. A. Li, F. M. Anastassacos, D. J. Mooney, W. M. Shih, *Nat. Commun.* **2017**, *8*, 15654.
- [53] M. Kuhlmann, J. B. R. Hamming, A. Voldum, G. Tsakiridou, M. T. Larsen, J. S. Schmökel, E. Sohn, K. Bienk, D. Schaffert, E. S. Sørensen, J. Wengel, D. M. Dupont, K. A. Howard, *Mol. Ther.–Nucleic Acids* **2017**, *9*, 284.
- [54] G. van Meer, A. I. P. M de Kroon, *J. Cell Sci.* **2011**, *124*, 5.
- [55] A. Moscho, O. Orwar, D. T. Chiu, B. P. Modi, R. N. Zare, *Proc. Natl. Acad. Sci. U. S. A.* **1996**, *93*, 11443.
- [56] C. Schneider, W. Rasband, K. Eliceiri, *Nat. Methods* **2012**, *9*, 671.
- [57] A. L. B. Pyne, A. Noy, K. H. S. Main, V. Velasco-Berrelleza, M. M. Piperakis, L. A. Mitchenall, F. M. Cugliandolo, J. G. Beton, C. E. M. Stevenson, B. W. Hoogenboom, A. D. Bates, A. Maxwell, S. A. Harris, *Nat. Commun.* **2021**, *12*, 1053.
- [58] P. J. Haynes, K. H. S. Main, B. Akpınar, A. L. B. Pyne, *Chromosome Architecture* **2022**, 43.
- [59] D. Nečas, P. Klapetek, *Open Phys. J.* **2012**, *10*, 181.
- [60] I. D. Bennett, J. R. Burns, M. G. Ryadnov, S. Howorka, A. L. B. Pyne, Lipidated DNA Nanostructures target and rupture bacterial membranes. The University of Sheffield. Dataset, <https://doi.org/10.15131/shef.data.25662963>.